INTERFACE

royalsocietypublishing.org/journal/rsif

Research

Cite this article: Morrissey SJ, Schlaefer JA, Jerry DR, Kingsford MJ. 2026 Estimating transport and detectability of *Chironex fleckeri* environmental DNA in an open coastal bay. *J. R. Soc. Interface* **23**: 20250354.
https://doi.org/10.1098/rsif.2025.0354

Received: 22 April 2025
Accepted: 5 December 2025

Subject Category:
Life Sciences–Earth Science interface

Subject Areas:
ecosystem, environmental science, computational biology

Keywords:
environmental DNA, Cubozoa, particle dispersion, detection, spatial detection limits, biophysical modelling

Author for correspondence:
Scott J. Morrissey
e-mail: scott.morrissey@my.jcu.edu.au

Electronic supplementary material is available online at https://doi.org/10.6084/m9.figshare.c.8262531.

THE ROYAL SOCIETY PUBLISHING

Estimating transport and detectability of *Chironex fleckeri* environmental DNA in an open coastal bay

Scott J. Morrissey[1,2], Jodie A. Schlaefer[5,3], Dean R. Jerry[1,6,4] and Michael J. Kingsford[1,2]

[1]Marine Biology and Aquaculture, College of Science and Engineering, [2]ARC Centre of Excellence for Coral Reef Studies, [3]The Centre of Tropical Water and Aquatic Ecosystem Research (TropWATER), and [4]ARC Research Hub for Supercharging Tropical Aquaculture through Genetic Solutions, James Cook University, Townsville, Queensland, Australia
[5]Department of Environment, Commonwealth Scientific and Industrial Research Organisation, Townsville, Queensland, Australia
[6]Tropical Futures Institute, James Cook University, Singapore, Republic of Singapore

SJM, 0000-0002-2416-3045

Environmental DNA (eDNA) has emerged as a powerful tool for species detection and monitoring; however, understanding its dispersion and transport dynamics and how this influences detectability is essential to enhance the accuracy of eDNA use. A biophysical model was used to investigate the spatiotemporal dispersion of *Chironex fleckeri* eDNA in an open coastal bay in northern Australia. The model revealed that local hydrodynamics, geomorphology and meteorological conditions shaped 'detection shadows', with eDNA detectability constrained from hundreds of metres to kilometres from seeding locations. These dispersion estimates are closely aligned with empirical detections of *C. fleckeri* medusae and polyps, demonstrating the utility of biophysical models for estimating eDNA transport and dispersal dynamics. The findings highlight the influence of eDNA decay and dilution on detectability and provide valuable insights for interpreting detections of targeted taxa. Here, we demonstrate the broader potential of combining biophysical modelling with eDNA sampling.

1. Introduction

Environmental DNA (eDNA) provides a non-invasive and efficient method to detect species within their environment [1,2]. It is increasingly being explored and applied as an ecological survey and management tool to further understand species' presence and distributions. Furthermore, it can provide critical information to stakeholders and decision makers surrounding the risk management of problematic species [3–7]. However, the accuracy of using eDNA as a detection method is at times questioned due to fundamental knowledge gaps surrounding the 'ecology' of eDNA [8,9], particularly its physical transport and dispersion within the natural environment [8,10]. This understanding is crucial for linking eDNA-based detections to the physical presence of taxa, thereby distinguishing between true detections and those arising from allochthonous eDNA. In this context, a 'true' detection is inherently scale- and context-dependent. It refers to eDNA originating from organisms within the relevant area of interest, rather than from adjacent habitats via transport. Thus, the interpretation of detections must consider both the spatial scale of interest and the hydrodynamic connectivity of the system. Current interpretations of eDNA-based species detections often rely on eDNA persistence times and thus temporal detection windows. However,

as highlighted by Thomsen *et al.* [11], eDNA has the potential to travel significant distances, ranging from tens to hundreds of kilometres before decaying. Therefore, understanding the spatiotemporal dispersion of eDNA is key for enhancing the accuracy of eDNA-based species detections and to inform efficient sampling strategies [10,12].

eDNA is largely at the mercy of hydrodynamic forces and meteorological conditions [10,13], which can vary significantly across environments. For instance, in still water environments, horizontal eDNA transport tends to be limited [14–16], with maximum distances reported to be only hundreds of metres from source individuals [15,17]. Conversely, in environments with actively flowing water, eDNA transport has been reported over distances ranging from kilometres [18–21] to tens of kilometres [22,23]. This dispersion is influenced by numerous extrinsic factors such as flow velocity and river characteristics/morphology [18,21]. Intrinsic factors such as eDNA decay rates, organism shedding rates and biotic and abiotic conditions may also influence these processes [24] and interact with extrinsic forces to shape eDNA transport dynamics. Given these interacting influences and found variability, detailed understandings of eDNA transport across differing environments and conditions are essential for interpreting eDNA-based detections.

In marine environments, these complexities are amplified due to the interplay of extrinsic factors, such as tides, water density, wind patterns, ocean currents, bathymetry and coastal geomorphology. These interactions create variable water movements, both horizontally and vertically, resulting in complex hydrodynamic conditions. As a result, the transport of eDNA in marine systems likely exhibits significant spatial variability. Empirical studies highlight this with reported maximum detection distances from known source individuals ranging from hundreds of metres to kilometres [13,25–31].

Biophysical modelling has been successfully utilied to investigate the transport and dispersal patterns of passive particles in marine systems for numerous applications [32–34]. Subsequently, it has been highlighted as a method to study the transport and dispersion of eDNA [10,35–38]. Recently, this approach has been utilized to examine eDNA transport and dispersal to inform and improve sampling designs [35,38,39] and to identify origin locations of eDNA [36,40]. With the incorporation of known eDNA degradation rates, it is possible for this approach to reveal and allow study of the spatiotemporal distribution of detectable eDNA from source individuals, termed ‘eDNA shadows’ by Ellis *et al.* [35]. This approach holds potential to enhance the interpretation of eDNA detections and the sampling effort required to maximize detections [35]. The use of biophysical models for this purpose generally lacks ground truthing. Accordingly, comparisons between modelled and measured eDNA concentrations need to be further explored in marine environments.

eDNA has recently been applied to detect and study problematic jellyfish, specifically the notorious Australian box jellyfish, *Chironex fleckeri* [41–43]. Morrissey *et al.* [41] displayed the efficacy of eDNA both in detecting major life history stages and in delineating population stock boundaries of the species [41,42]. Using a grid sampling design within an open coastal bay (Horseshoe Bay of Magnetic Island, Australia), they determined the nearshore distribution of the species, with detections exclusively at nearshore sites and with non-detections at sites located hundreds of metres to kilometres from shore across multiple sampling times [42]. Based on these findings, they suggested that *C. fleckeri* eDNA dispersal is likely limited and recommended use of biophysical models to test this hypothesis. This presented an opportunity to utilize biophysical models to evaluate the spatiotemporal dispersal potential of eDNA within an open coastal bay and to compare modelled eDNA transport with empirical data [42]. Accordingly, this study could aid in the monitoring and management of a deadly species and offer insights into eDNA dispersal dynamics in open coastal embayments.

The objective of this study was to utilize biophysical models to examine the transport of *C. fleckeri*’s eDNA within an open coastal bay under varying conditions, to improve our understanding of the relationship between species presence and eDNA detections. Specifically, we aimed to determine the following: (i) oceanographic and meteorological influences upon eDNA transport and dispersion in an open coastal bay, (ii) spatiotemporal dispersion of simulated eDNA, to better understand how long and at what spatial scale eDNA signals remain viable for detection, and (iii) how modelled transport and estimates of detection limits compare with empirical field detections of *C. fleckeri*.

2. Material and methods

2.1. Study area

This study encompassed an open coastal bay, Horseshoe Bay, Magnetic Island, Australia (19.11° S, 146.85° E). Horseshoe Bay is an approximately 2.5 by 1.7 km shallow bay, buffered by rocky headlands, with a maximum depth of approximately 10 m (figure 1). The bay has a sandy beach environment, with some fringing seagrass beds and coral reef, and a tidally isolated freshwater inflow located in its southeast corner. It has an average tidal range of approximately 3.4 m, and the water column is generally unstratified [42]. This area was selected due to the availability of empirical data on detections of *C. fleckeri* eDNA [42].

2.2. Study species

Chironex fleckeri, the Australian box jellyfish, is a highly venomous species found along the northern coast of Australia from Gladstone to Broome, extending into the Indo-Pacific [44]. The species has a polymorphic life history where its medusae stage is seasonal (Austral summer; October to May) [45,46]. This stage is known to maintain a nearshore distribution in Australia [42,47,48], and the medusae and polyp stages of this species are specifically known to be present within Horseshoe Bay [42]. Medusae were exclusively detected along the shore of the bay, while polyps were putatively detected within the eastern tidally isolated freshwater inflow of the bay (figure 1) [42]. The seasonal separation of these life history stages, with medusae occurring

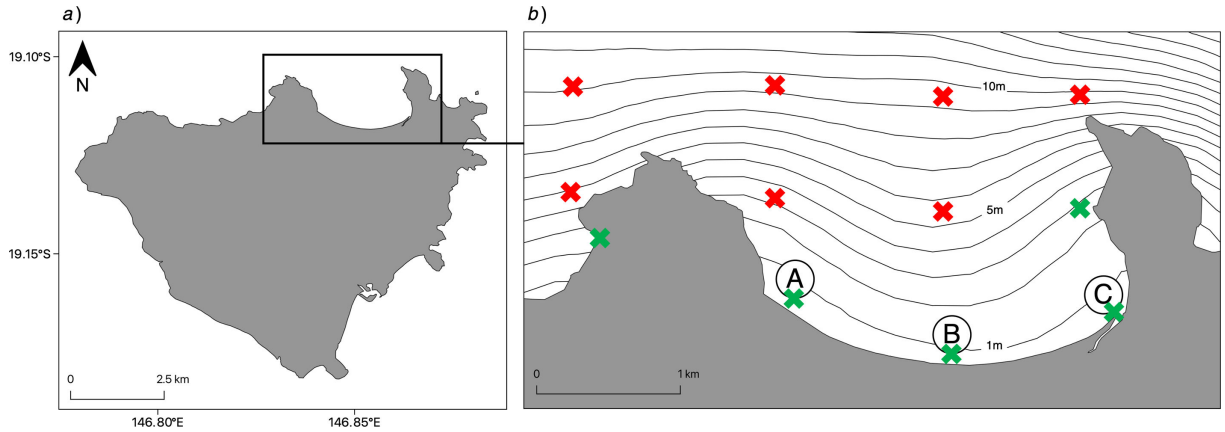

Figure 1. Study site. (*a*) Magnetic Island, and (*b*) map of Horseshoe Bay with bathymetry of the bay (1 m interval contour lines) and particle seeding locations (A, B, C). Outside of the Australian stinger season, particle seeding location is C. Green crosses are indicative of empirical positive field detections of both medusae and polyps, and red crosses are indicative of negative field detections as per Morrissey *et al.* [42].

in waters from September to May and polyps persisting during winter months when medusae are absent, enables their respective detection via eDNA [41,42]. This ecological knowledge was utilized to inform the approach to modelling (§2.4.1).

2.3. Biophysical model

2.3.1. Hydrodynamic model

The depth-averaged currents around Magnetic Island were simulated using the two-dimensional (2D) version of the Second-generation Louvain-la-Neuve Ice-Ocean Model (SLIM2D) [49]. SLIM2D was selected due to the bay's shallow, well-mixed waters, where eDNA is likely to be mixed throughout the water column [42,50]. Moreover, SLIM2D has previously been effectively utilized in accurately simulating the hydrodynamics of shallow systems [49,51].

The model domain extended far enough to (i) include key oceanographic processes that can influence the currents around Magnetic Island and (ii) avoid confounding open boundary errors. Specifically, the model domain encompassed an area from the middle of the Queensland Plateau to the far south of Magnetic Island, extending from the Queensland coast out into the Coral Sea (electronic supplementary material, figure S1), as per the domain utilized by Schlaefer *et al.* [51]. Thereby, the domain captured the interactions of the North Caledonian Jet of the South Equatorial Current with the continental shelf south of the Queensland Plateau [52,53].

In SLIM2D, the depth-averaged shallow-water equations are solved for sea surface elevation and zonal (west to east) and meridional (south to north) current components. The equations are discretized spatially using a second-order discontinuous Galerkin finite element method and temporally using a second-order implicit Runge–Kutta method [49]. Importantly, because of the method of spatial discretization, we could use an unstructured grid. Our unstructured grid has coarser elements in open water and finer elements near coasts and reefs, with the greatest resolution at our study location of Horseshoe Bay (electronic supplementary material, figure S1). This grid contained 68 403 triangles with side lengths ranging from 25.90 m nearshore to 7.75 km offshore. Each triangle has three degrees of freedom (i.e. there were three axes along which the variable could translate), so there were 68 403 × 3 = 205 209 degrees of freedom in total. The variation in triangle size enabled us to have a computationally efficient model that could represent both the large-scale oceanographic influences on Magnetic Island and the fine-scale flows around complex bathymetry (i.e. coastlines).

We used a standard model set-up. Sea surface elevation and zonal and meridional current components were prescribed at the open boundaries on the outside of the model domain, and wind was prescribed over the entire domain. Tide and current data were sourced from eReefs GBR 4 [54], and wind data from the Australian Bureau of Meteorology's (BoM) Atmospheric high-resolution Regional Reanalysis for Australia [55]. Additionally, bottom friction dissipation was computed using a Chezy–Manning scheme, incorporating the Chezy–Manning–Strickler formulation, which accounts for drag as water flows over the seabed. Finally, turbulent viscosity, an important parameter in eddy simulation, was determined through a Smagorinsky scheme.

The hydrodynamic model was run for four distinct time periods: two within the Australian box jellyfish season (October 2016 to January 2017 and October 2017 to January 2018) and two outside of the season (June to September 2017 and June to September 2018). The hydrodynamic fields were simulated every 3 min and saved every 30 min. This high temporal resolution was utilized to match the fine-scale resolution of the SLIM grid to ensure that complex coastal hydrodynamic features were effectively simulated.

2.3.2. Hydrodynamic model validation

The fine-scale hydrodynamics at the study location were well represented in the hydrodynamic model. The model was validated through comparisons to measured tidal anomalies for the area from a local tidal gauge (Maritime Safety Queensland, Queensland Government) and to water current data collected in Horseshoe Bay at five sites from November 2017 to January

2018 through use of drag-tilt current meters (electronic supplementary material, figure S2). The skill in modelling water level anomalies and zonal and meridional current components was assessed through data visualizations and calculation of the normalized root mean square error of the simulated versus observed data (electronic supplementary material, figure S3 and tables S1 and S2). Further details can be found in electronic supplementary material, 1.1.

2.4. Simulating environmental DNA particle transport

2.4.1. Particle releases

The transport of passive virtual eDNA particles was simulated by coupling the SLIM Lagrangian particle tracker model with the hydrodynamic model [49,56]. Herein, 'particle' refers to a computational parcel of eDNA mass rather than a discrete cell or fragment. In the Lagrangian particle tracker, the particles were dispersed based on the currents simulated by the hydrodynamic model at the grid scale and by horizontal diffusivity from turbulent mixing at the sub-grid scale. The horizontal diffusivity was parametrized as a function of the local grid cell size using an Okubo scheme following de Brye *et al.* [57].

Initial particle release concentrations were determined from empirical field concentrations [42]: 200 copies l^{-1} during the stinger season, and 100 copies l^{-1} outside of it. These concentrations reflect the approximate maximum concentration of *C. fleckeri* eDNA captured during and outside of the Australian stinger season, respectively [42]. This approach enhanced the ecological relevance of the simulations, ensuring that the modelled concentrations more accurately reflected real-world conditions and the sensitivity of the utilized workflow [43]. To produce these concentrations, the numbers of particles released ranged from 364 477 to 900 773. Although no sensitivity analysis has been conducted on the requirements to model eDNA dispersal, these numbers were three orders of magnitude greater than the number of particles required to robustly represent the dispersal of marine plants in a similar environment [58]. Particle releases during the Australian stinger season occurred from three locations (figure 1). This was undertaken to mirror the known presence and movements of *C. fleckeri* medusae along the shore of Horseshoe Bay, which allowed for a spatially variable eDNA source region [42]. Conversely, only a single location was utilized outside of the Australian stinger season to reflect where *C. fleckeri* polyps were putatively detected within Horseshoe Bay (figure 1). A decay function, consistent with known *C. fleckeri* eDNA decay [43], was applied to the particles post-release. This function employed three differing decay rates to reflect the various observed stages of particle decay [43]. Use of this decay function, instead of a first-order decay model that may oversimplify this process [9], aids in recreating real-world eDNA 'behaviour' and provides a more accurate representation of eDNA persistence [36]. This decay function aligned well with observed decay data [43] through use of a regression analysis (slope = 0.99, intercept = 0.047, $R^2 = 0.99$, $p < 0.01$). To ensure robustness, the decay function was applied five replicate times upon each particle release, with randomly selected particles to be decayed, to capture any potential variation in particle transport. This approach allowed for a more accurate assessment of variability in dispersion patterns, ensuring that the results reflected a range of possible particle decay scenarios. Particles were released from each seeding location every 10 h over a 7 day simulation period.

2.4.2. Tidal and wind conditions

The influence of two varying tidal and wind conditions on eDNA transport was examined. Regarding tidal conditions, spring and neap tidal phases were chosen as they represent the two extremes of the tidal regime. For wind conditions, southeasterly (SE) and northeasterly (NE) conditions were selected, being the most common for the study area as per the Australian BoM's wind data for the Townsville region [59]. A combination of tidal and wind conditions resulted in four scenarios (table 1 and electronic supplementary material, figure S4), for both during and outside of the Australian stinger season. These scenarios were utilized to ensure a range of environmental conditions, potentially resulting in variable eDNA transport and dispersion, were comprehensively represented.

2.4.3. Particle transport analysis

To explore passive virtual eDNA transport, several methods were utilized. Firstly, particle locations were visualized on map charts for every hour post-release. The map charts were further combined to create animations to effectively visualize temporal changes in particle movement patterns. Next, an analysis of particle distribution within and outside of Horseshoe Bay through use of a defined geographical boundary box was undertaken. Boundaries were set as per electronic supplementary material, figure S5, and the average relative abundance of particles over time within and outside of Horseshoe Bay was calculated. Additionally, particle distance travelled, in relation to the initial seeding location, was calculated for all particles at each hourly timestep.

2.5. Comparison of simulated environmental DNA particle transport to field measurements

To compare simulated eDNA particle transport with empirical field measurements [42], log-normalized relative concentration map plots were created from the simulations. These plots accumulated particle positions across the entire dispersion time for all releases ($n = 17$), averaging the five decay scenario replicates, allowing for the visualization of relative particle concentrations. These plots were created using a 2D histogram approach, in which the study area was divided into a grid of 1 m^2 cells. The 1 m^2 cells were utilized to capture fine-scale dispersion patterns and to align the results with practical sampling areas where

Table 1. Conditions for tidal and wind scenarios, including tidal phase, average wind direction, average wind speed, timing in regard to the Australian stinger season and start and end date of each scenario.

scenario	tidal phase	average wind direction	average wind speed ($km\ h^{-1}$)	Australian stinger season	start date	end date
A	spring	123.3° (SE)	28.2	during	17 Jan 2018	23 Jan 2018
B	spring	43.4° (NE)	19.6	during	26 Dec 2017	1 Jan 2018
C	neap	126° (SE)	24.4	during	24 Jan 2018	30 Jan 2018
D	neap	45° (NE)	16.9	during	29 Dec 2016	4 Jan 2017
E	spring	142.7° (SE)	25.7	outside	28 Jun 2018	4 Jul 2018
F	spring	48.9° (NE)	12.3	outside	20 Sep 2017	26 Sep 2017
G	neap	145.9° (SE)	26.5	outside	20 Jun 2018	26 Jun 2018
H	neap	55° (NE)	18.7	outside	28 Sep 2017	4 Oct 2017

samples would be taken. Particle positions were aggregated over the entire simulation period, and the number of particles in each cell was recorded. A log-normalization was applied to enhance the visibility of regions with lower particle concentrations. The log-normalized counts were subsequently scaled so that the maximum particle concentration corresponded to a value of 1. A threshold of <1 particle per grid cell was applied to exclude cells with only transient, one-off particle pass-throughs, ensuring the plots reflect ecologically meaningful dispersal patterns rather than momentary artefacts of particle movement. A custom colour map was utilized to enhance visual interpretation, transitioning from blue for low-concentration areas (indicating particles below the detection limit) to yellow at the detection limit, and red for regions of high particle concentrations. A rapid transition at the detection limit was used to highlight areas of particular interest.

3. Results

3.1. Hydrodynamics of Horseshoe Bay

The hydrodynamic model of Horseshoe Bay revealed complex circulation driven by tidal currents and influenced by the bay's geomorphology (electronic supplementary material, animation S1–S4). Tidal jets entered on the western side during ebb tides and the eastern side during flood tides, creating dynamic flows that bifurcated upon entering the bay. This formed gyre-like circulation patterns within the bay and shore-parallel currents. Slower currents occurred nearshore, while faster flows around the rocky headlands enhanced circulation and flushing in the bay's central area. Eddies formed near the headlands and along the bay's periphery due to interactions between tidal jets and slower coastal waters, additionally creating free shear layers. The eastern section of the bay, sheltered by the headland, experienced slower flows, resulting in a general area of 'sticky water' [60]. These patterns highlighted the spatial variability of water movement throughout Horseshoe Bay.

3.2. General transport patterns of environmental DNA within an open coastal bay

The dispersion of eDNA displayed two main behaviours. Initially, particles remained near the shore, transported by shore-parallel currents. Upon leaving the bay or moving offshore, they were quickly advected from the bay by reversing tidal flows and dispersed broadly (figure 2; electronic supplementary material, figures S6–S13 and animation S5–S12). Currents within and bordering the bay clustered particles in specific areas, particularly along the sides and periphery of the bay, where eddy currents created transient aggregations which alternated between being further and closer to seeding locations with tidal oscillations (figure 2). Tidal flows additionally caused oscillating particle movement within the bay where ebb tides generally transported particles away from seeding locations, while flood tides brought them closer. While particles from all seeding locations displayed similar behaviours, their trajectories varied. Those from the eastern side of the bay (seeding location C) generally travelled along the eastern headland, while those from the central and western side of the bay (seeding locations B and A) followed the shore and western headland. These transport patterns were consistent during and outside of the Australian stinger season.

3.3. Retention and transport of environmental DNA

There was great spatial variation in particle retention across the bay where hydrodynamic and meteorological conditions played a role. During the Australian stinger season, for all scenarios, particle presence within the bay dropped below 1% within 21–25 h

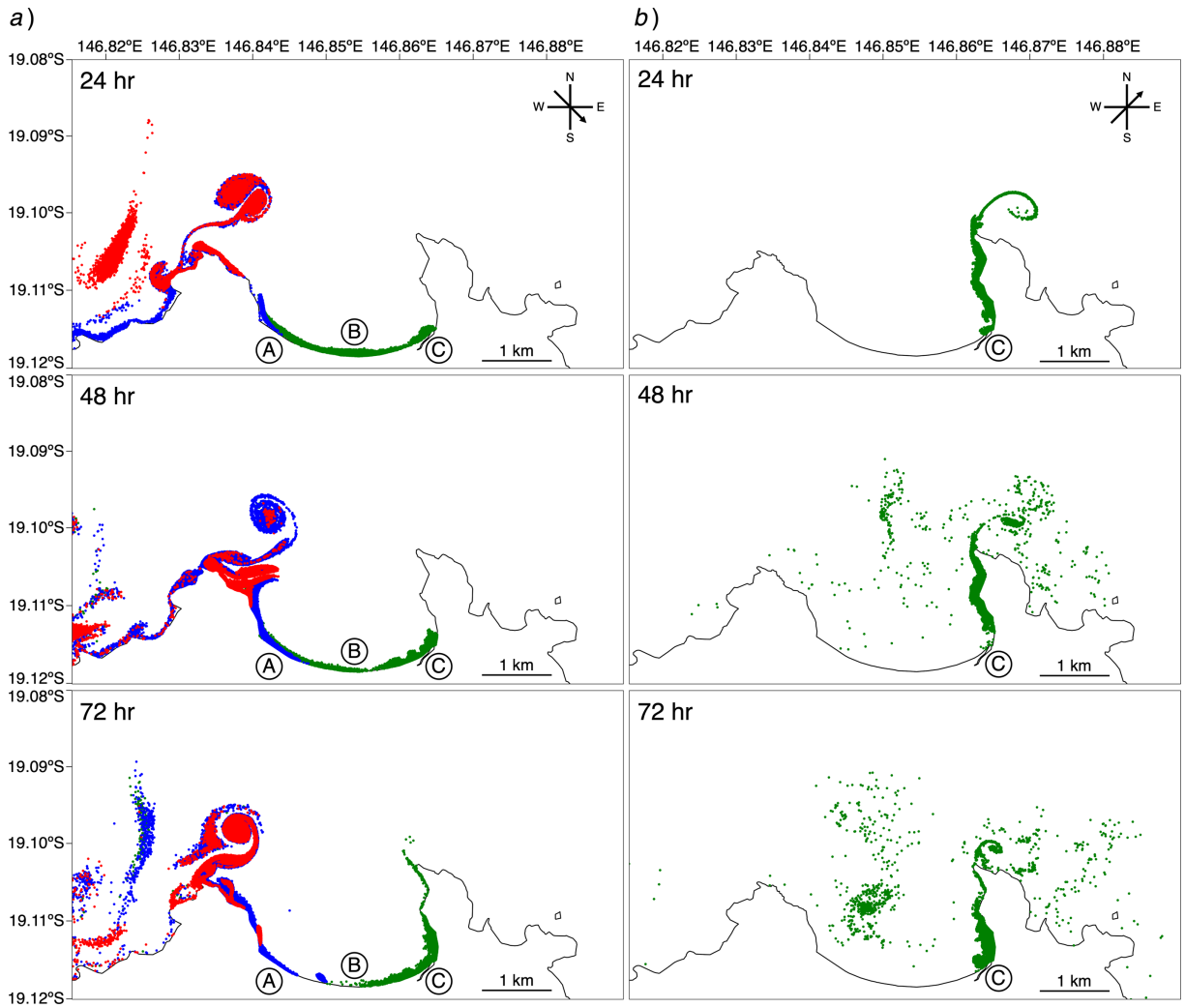

Figure 2. Maps of Horseshoe Bay displaying simulated eDNA particle transport at 12, 24 and 72 h intervals (*a*) representative of medusae, during spring tide and SE wind conditions (scenario A), and (*b*) representative of polyps, during spring tide and NE wind conditions (scenario F). Red particles were released from location A, blue from location B and green from location C. Wind direction arrows in the 24 h panels indicate the direction of the wind in both scenarios.

post-release, with only 1.24–9.87% of particles actually exiting the bay, suggesting a rapid daily turnover largely resulting from eDNA decay. Retention varied by seeding location (table 2), where particles from the eastern side (location C) exhibited the longest retention times (<1% at 26 h) and minimal transport outside the bay (<1%), highlighting their persistence within this area and the dominance of decay on particles in low-energy regions. Those from the western side (location A) exhibited the shortest retention, followed by central particles (location B), where spring tides increased particle export while neap tides enhanced retention. However, wind direction had a stronger influence than tide, where SE winds reduced particle retention regardless of tidal phase. Outside of the stinger season, similar patterns occurred, with particles again being retained within the eastern side of the bay (<1% at 26 h). Data on particle transport distances from seeding locations can be found in electronic supplementary material, 4.0.

3.4. Spatiotemporal distribution and detectability of simulated environmental DNA particles

Particles outside of the bay were generally estimated to be below detection limits, aligning with empirical detections (figure 3). Across all scenarios, the highest particle concentrations occurred near seeding locations and nearshore within the bay. Particle concentrations decreased with increasing distance from the seeding locations, reflecting the combined effects of particle dilution and decay. This decline spanned hundreds of metres to kilometres alongshore. Moving perpendicular from shore, this decline was more rapid, highlighting the retention of particles nearshore.

Under SE winds (figure 3*a*,*c*), the dispersion of detectable particles was tighter and more concentrated nearshore within the bay, while under NE winds (figure 3*b*,*d*), particles displayed a broader perpendicular spread. The eastern side of the bay (seeding location C) exhibited the broadest and most sustained particle concentrations, again showing that particles persisted longer in this area compared to other locations (figures 3 and 4). Eddy-like patterns were discernible in all plots (figures 3 and 4), indicating that particles were temporarily trapped by this oceanographic phenomenon when exiting the bay. However, these particles were present at low concentrations, below the detection limit. An exception occurred outside and west of the bay where particles were estimated to be present at detectable levels in some areas. Despite some variation in the spatial distribution of particles across scenarios, general trends remained consistent and aligned well with empirical *C. fleckeri* eDNA detections, which were restricted to nearshore locations [42].

Table 2. Time at which the average relative abundance of particles within Horseshoe Bay dropped below 1% and the maximum average relative abundance of particles transported outside of the bay during the simulation period. Values represent the median of each particle release ($n = 16$), with the range shown in parentheses. Results are presented for each location individually and for combined locations, across scenarios.

scenario	tidal phase	wind direction	location	<1% (h)	maximum outside (%)
A	spring	SE	A	8 (4–16)	28.89 (8.31–57.29)
			B	14.5 (6–22)	8.34 (0–37.3)
			C	26 (26–26)	0.02 (0–0.36)
			combined	21 (20–24)	9.87 (2.31–26.06)
B	spring	NE	A	17 (6–26)	5.67 (0–39.41)
			B	23 (15–26)	1.11 (0–7.68)
			C	26 (26–26)	0.01 (0–0.06)
			combined	24 (20–26)	2.21 (0–10.63)
C	neap	SE	A	10 (4–18)	21.46 (0–71.81)
			B	18 (6–26)	3.54 (0–37.15)
			C	26 (20–26)	0.10 (0–1.84)
			combined	21 (20–24)	6.01 (0–26.03)
D	neap	NE	A	22 (6–26)	3.04 (0.02–39.84)
			B	26 (14–26)	0.12 (0–7.72)
			C	26 (26–26)	<0.01 (0–0.1)
			combined	25 (20–26)	1.24 (0–10.74)
E	spring	SE	C	26 (19–26)	0.05 (0–2.75)
F	spring	NE	C	26 (23–26)	0 (0–0.82)
G	neap	SE	C	26 (24–26)	0.38 (0–0.69)
H	neap	NE	C	26 (26–26)	0.01 (0–0.08)

4. Discussion

4.1. Hydrodynamic and meteorological drivers of environmental DNA transport

This study highlights the necessity of location-specific understandings of hydrodynamic and meteorological drivers of eDNA transport. Specific hydrodynamic characteristics and localized conditions within Horseshoe Bay produced varied transport pathways and spatially heterogeneous eDNA distribution patterns, emphasizing the scale-dependent nature of eDNA transport and its contingency on localized conditions. The simulations revealed the presence of free shear layers, which limit cross-boundary particle movements [61], reversing tidal flows and shear-induced eddy currents, which drove specific and varied transport pathways. These oceanographic phenomena resulted in alongshore transport, rapid advection, transient aggregations of particles in particular areas of the bay and hence controlled the bulk transport of simulated eDNA particles. Additionally, the bay's geomorphology resulted in an area of 'sticky water' [60], defined as a zone of reduced flow and circulation, along the eastern shoreline and headland, which resulted in variable retention rates of particles across the bay. Meteorological conditions, specifically wind direction, also modulated these transport and retention patterns, with SE winds promoting offshore currents and reduced retention, while NE winds enhanced retention by slowing offshore flows. This effect of wind upon eDNA transport has previously been observed by Rollan *et al.* [38], where an introduced eDNA signal was largely influenced by wind-driven surface currents. Clearly, the interplay of three major extrinsic factors was driving eDNA transport.

Marine systems, whether distinctive, like semi-enclosed bays and open ocean environments, or similar, such as embayments of various sizes and morphologies, likely demonstrate distinctive eDNA transport characteristics dictated by their unique hydrodynamics and localized conditions. For instance, Ellis *et al*. [35] showed, through biophysical models, that open coastline systems often exhibit greater alongshore eDNA transport than cross-shelf; however, this varies with each system's exposure to regional hydrodynamic forces. Similarly, Wolanski *et al*. [56] showed, again through biophysical models, that passive particles (representing coral larvae) exhibited differing degrees of retention within embayments due to variations in their morphology and exposure to prevailing hydrodynamic forces. This study provides a finer-scale examination of the factors responsible for eDNA transport and showcases significant spatial variability, highlighting the importance of such understandings for the interpretation of eDNA detections.

4.2. Spatiotemporal dispersion and detectability of environmental DNA

Incorporation of the detection threshold of the *C. fleckeri*-specific assay [43], with eDNA transport dynamics, described above, indicated that *C. fleckeri* eDNA remained detectable from hundreds of metres to kilometres from sources. These spatially

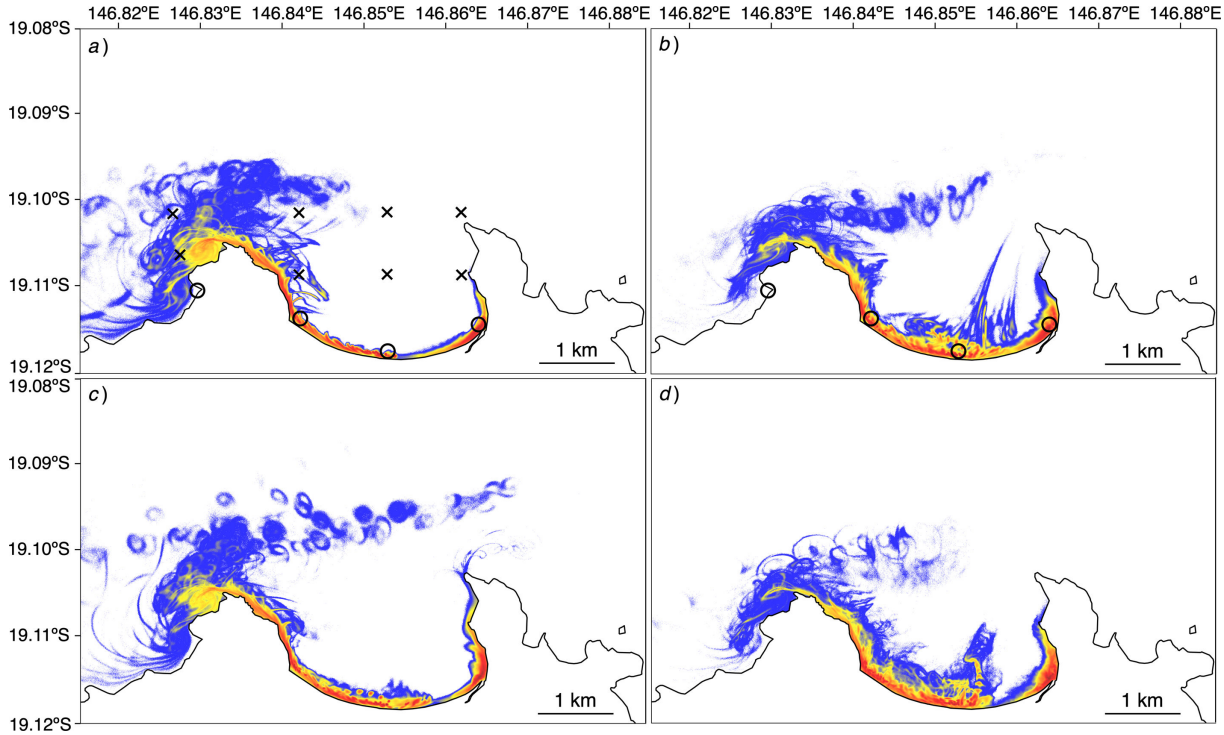

Figure 3. Log-normalized relative simulated eDNA particle concentrations from *C. fleckeri* medusae for (*a*) spring tide, SE winds (scenario A); (*b*) spring tide, NE winds (scenario B); (*c*) neap tide, SE winds (scenario C); and (*d*) neap tide, NE winds (scenario D) during the Australian stinger season. Plots show cumulative relative particle concentrations over time. Red to yellow colours indicate concentrations above detection limits; blue colours represent those below. Circles indicate positive empirical *C. fleckeri* medusae detections, and crosses indicate negative detections, shown only on plots matching empirical sampling conditions (electronic supplementary material, table S3).

small 'detection shadows' were largely confined to the bay, shaped by eDNA decay, particle dilution and transport dynamics, which limited the detectability of simulated eDNA. Environmental conditions within Horseshoe Bay, notably water temperature (29–33.8°C) [42], are suitable for relatively rapid decay of *C. fleckeri* eDNA. Experimental work on this species [43] shows that *C. fleckeri* eDNA decays rapidly, reaching low levels after approximately a day. When combined with the short water residence time in the bay, this suggests that detectable eDNA reflects recent shedding and therefore local and current presence, rather than long-distance persistence or transport. Some particles, despite decay, travelled significant distances from sources; however, they were unlikely to be detected due to their low density. Detecting these particles would require collecting and filtering hundreds of litres of water. Consequently, *C. fleckeri* eDNA exhibited rapid spatial and temporal turnover, with detectable signals persisting for only short periods, likely on a daily scale. Thus, eDNA-based detections of *C. fleckeri* likely reflect the species' close proximity and current presence [42], reinforcing eDNA's value as an ecological survey [41,42] and potential management tool for cubozoans.

Similar findings have been reported by Ellis *et al.* [35], who also utilized biophysical models to explore 'detection shadows' of invasive *Undaria pinnatifida* (wakame) and *Asterias amurensis* (North Pacific sea-star), which ranged between 1 and 3 km in size, with *in situ* sampling providing additional support. Numerous field-based studies have also reported that eDNA detections are typically confined to distances of hundreds of metres to a few kilometres from source individuals [13,25,29]. These findings, along with the present study, add to increasing evidence of a high site fidelity of eDNA to its source in marine environments [10]. However, spatial inconsistencies in detections surrounding known source individuals [13,62] do highlight the importance of understanding eDNA transport dynamics for interpreting detections. Murakami *et al.* [13] reported inconsistent detection along transects leading from juvenile *Pseudocaranx dentex* (striped jack) in a sea cage where occasional absences were found, even at nearby sampling distances. Further, Strickland *et al.* [62], through undertaking an encircling sampling array around individual *Malo bella* medusae, found inconsistent detection at close distances. These spatial inconsistencies are likely a result of small-scale eDNA trails that were yet to disperse. Accordingly, understanding of eDNA dispersal in a species-specific and environmental context would be beneficial for determining the potential for false negative detections, particularly in scenarios where rapid eDNA decay or dilution may reduce detection probability.

These insights have practical implications for detecting *C. fleckeri*. Given the species' nearshore residence [47,63,64] and the confinement of eDNA signals to nearshore areas, a targeted shoreline sampling strategy may enhance detection success. Additionally, as *C. fleckeri* is generally a species of low abundance [41], eDNA may help distinguish its presence between neighbouring bays and sampling locations, aiding in assessing localized risk to water users [46]. Furthermore, this may allow for the assessment of medusae movements between locations, an area of research where direct observations are challenging [45,65], which would be beneficial to understandings of population connectivity [44]. The rapid spatial and temporal turnover of *C. fleckeri* eDNA showcases the time-sensitive nature of detections, reinforcing eDNA's value as a precise and cost-effective tool for ecological surveys and risk management.

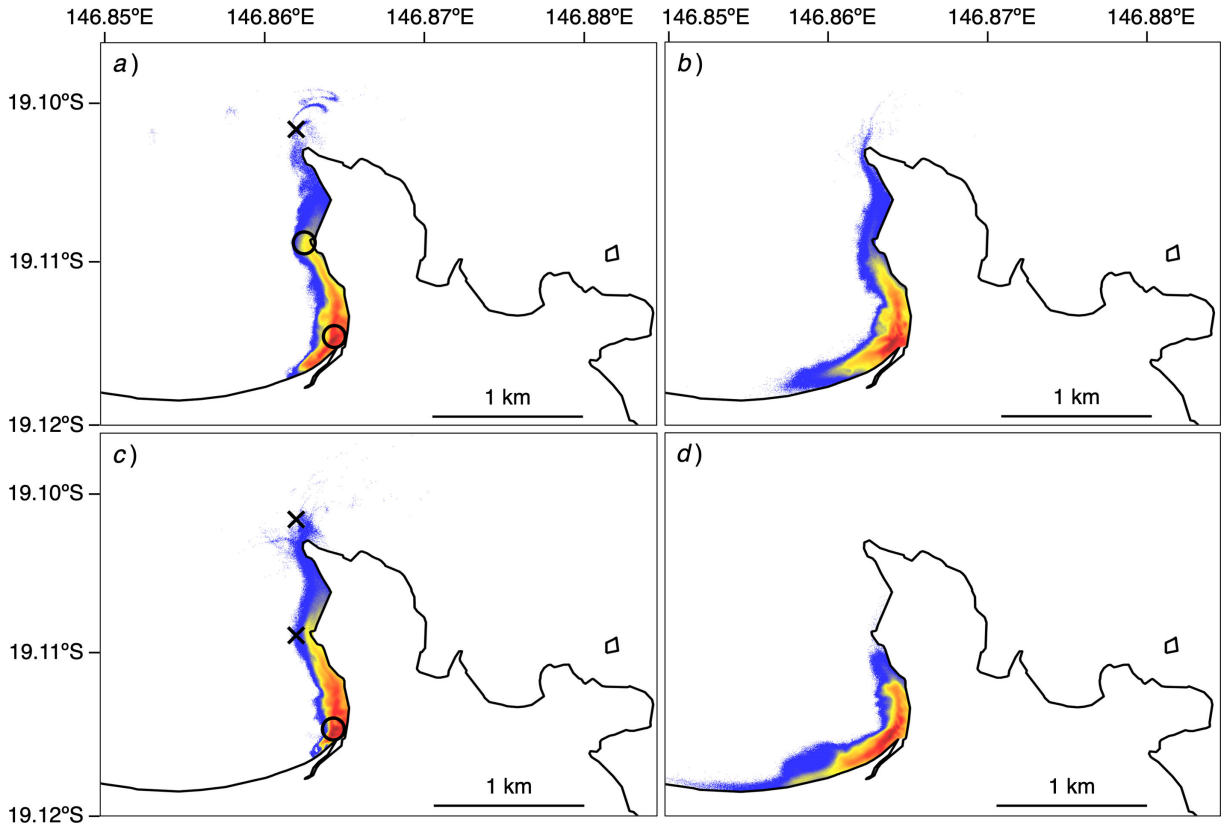

Figure 4. Log-normalized relative simulated eDNA particle concentrations from *C. fleckeri* polyps for (*a*) spring tide, SE winds (scenario E); (*b*) spring tide, NE winds (scenario F); (*c*) neap tide, SE winds (scenario G); and (*d*) neap tide, NE winds (scenario H) outside the Australian stinger season. Plots show cumulative relative particle concentrations over time. Red to yellow colours indicate concentrations above detection limits; blue colours represent those below. Circles indicate positive empirical *C. fleckeri* polyp detections, and crosses indicate negative detections, shown only on plots matching empirical sampling conditions (electronic supplementary material, table S3).

4.3. Comparison of modelled transport with empirical *Chironex fleckeri* detection

The simulated 'detection shadows' of *C. fleckeri* eDNA showed strong alignment with positive empirical field detections of both *C. fleckeri* medusae and polyps [42]. Empirical non-detections at mid- and offshore locations, where simulated particles were present but at theoretical concentrations below the detection limit, further reinforce this alignment. In areas where eddies created transient aggregations of particles, potentially increasing local concentrations to detectable levels, empirical detections of *C. fleckeri* eDNA would have been expected as sampling was conducted across multiple times, under varying conditions. But understandably, negative detections aligned with model predictions where simulated eDNA was below detection limits. As *C. fleckeri* medusae are known to reside nearshore [42,47,48], the low simulated eDNA concentrations in mid- and offshore areas are consistent with expectations based on the species' presence and distribution. This agreement between modelled and empirical patterns highlights the ecological validity of the simulations and, in turn, supports the use of biophysical models to investigate eDNA transport dynamics. This study hence provides additional support to these combined approaches for investigating this aspect of eDNA 'ecology' [35,36,38].

4.4. Limitations, considerations and future directions

This study has demonstrated the considerable value of biophysical models combined with field sampling in revealing the transport dynamics and spatiotemporal detectability of C. *fleckeri* eDNA within a dynamic open coastal embayment. However, like any modelling approach, certain methodological considerations and limitations shape the interpretation of findings and should be addressed here. One key limitation is the challenge of representing eDNA behaviour in all its complexity. The model utilized in this study treated eDNA as passive particles, thereby neglecting processes such as aggregation, sinking or interactions with suspended matter [10,66,67]. Furthermore, eDNA exists across a broad range of particle-size fractions, from free extracellular DNA to whole cells and mucus-bound aggregates [68]. Differences in buoyancy and degradation rates [69] among these fractions may influence their respective transport. These factors may therefore alter dispersal patterns, potentially leading to an overestimation of detectable eDNA signals within this study [10]. The sinking of particles was not considered in this study due to the well-mixed nature of the bay [42] and the unavailability of data on the specific gravity of eDNA.

The focus on eDNA detectability in this study also raises important considerations. As eDNA detection techniques become increasingly sensitive, such as with the adoption of digital PCR and CRISPR (clustered regularly interspaced short palindromic repeats) based assays [5,70], detectable signal ranges may expand. Without corresponding knowledge of eDNA transport dynamics, these advances may complicate the interpretation of the source of eDNA for ecological survey applications. A

clear understanding of spatiotemporal eDNA patterns, tailored to the sampling workflow, is essential to ensure accurate interpretation of eDNA data. To further advance understanding of eDNA transport dynamics, future studies should explore this in other environmental contexts. These efforts would refine our understanding of the factors influencing eDNA dispersal and detectability.

5. Conclusion

This study demonstrates the utility of biophysical models combined with field sampling in understanding eDNA transport and dispersion within a dynamic marine environment. Furthermore, modelling reveals the critical role of hydrodynamics, geomorphology and meteorological conditions in shaping spatially constrained eDNA 'detection shadows'. By incorporating species-specific eDNA parameters, the model closely aligned with empirical detections of *C. fleckeri*, hence providing a robust framework for interpreting eDNA patterns and optimizing sampling strategies. These findings highlight the importance of environment-specific understandings for eDNA sampling, particularly in systems influenced by complex hydrodynamic forces. Without field measurements, modelled levels of dispersal could be exaggerated, emphasizing the value of empirical validation when applying biophysical models to explore eDNA dispersion. While this study focused on an open coastal bay, future research should extend these methods to varied marine contexts and incorporate additional factors, such as more complex eDNA dynamics, to further refine this understanding. Overall, this study not only advances our understanding of eDNA transport dynamics but also demonstrates the broader potential of combining biophysical modelling with eDNA techniques to enhance interpretations of eDNA-based species detections, to improve sampling strategies and to better understand the relationship between detections and the present location of target organisms.

Ethics. This work did not require ethical approval from a human subject or animal welfare committee.

Data accessibility. The code and data associated with this study can be found on Zenodo [71]. Additional information and Python scripts related to SLIM are available via the SLIM Project repository: https://git.immc.ucl.ac.be/slim/slim/-/wikis/home.

Electronic supplementary material is available online [72].

Declaration of AI use. We have not used AI-assisted technologies in creating this article.

Authors' contributions. S.J.M.: conceptualization, data curation, formal analysis, funding acquisition, investigation, writing—original draft, writing—review and editing; J.A.S.: conceptualization, methodology, resources, software, supervision, writing—review and editing; D.R.J.: conceptualization, supervision, writing—review and editing; M.J.K.: conceptualization, supervision, writing—review and editing.

All authors gave final approval for publication and agreed to be held accountable for the work performed therein.

Conflict of interests. We declare we have no competing interests.

Funding. Funding for the project was provided by the Australian Lions Foundation for Scientific and Medical Research on Marine Species Dangerous to Humans to S.J.M.

Acknowledgements. We thank Jonathan Lambrechts for advice and assistance with troubleshooting SLIM. We also thank the reviewers and Megan Moran for commenting on drafts of this paper. Finally, we acknowledge the Traditional Owners (past, present and emerging) of the lands where this project was carried out.

References

1. Beng KC, Corlett RT. 2020 Applications of environmental DNA (eDNA) in ecology and conservation: opportunities, challenges and prospects. *Biodivers. Conserv*. **29**, 2089–2121. (doi:10.1007/s10531-020-01980-0)
2. Thomsen PF, Willerslev E. 2015 Environmental DNA—an emerging tool in conservation for monitoring past and present biodiversity. *Biol. Conserv*. **183**, 4–18. (doi:10.1016/j.biocon.2014.11.019)
3. Simpfendorfer C, Kyne P, Noble T, Goldsbury J, Basiita R, Lindsay R, Shields A, Perry C, Jerry D. 2016 Environmental DNA detects critically endangered largetooth sawfish in the wild. *Endang. Species. Res*. **30**, 109–116. (doi:10.3354/esr00731)
4. Eva B, Harmony P, Thomas G, Francois G, Alice V, Claude M, Tony D. 2016 Trails of river monsters: detecting critically endangered Mekong giant catfish *Pangasianodon gigas* using environmental DNA. *Glob. Ecol. Conserv*. **7**, 148–156. (doi:10.1016/j.gecco.2016.06.007)
5. Uthicke S, Lamare M, Doyle JR. 2018 eDNA detection of corallivorous seastar (*Acanthaster cf. solaris*) outbreaks on the Great Barrier Reef using digital droplet PCR. *Coral Reefs* **37**, 1229–1239. (doi:10.1007/s00338-018-1734-6)
6. Doyle JR, McKinnon AD, Uthicke S. 2017 Quantifying larvae of the coralivorous seastar *Acanthaster cf. solaris* on the Great Barrier Reef using qPCR. *Mar. Biol*. **164**, 176. (doi:10.1007/s00227-017-3206-x)
7. Villacorta-Rath C, Adekunle AI, Edmunds RC, Strugnell JM, Schwarzkopf L, Burrows D. 2020 Can environmental DNA be used to detect first arrivals of the cane toad, *Rhinella marina*, into novel locations? *Environ. DNA* **2**, 635–646. (doi:10.1002/edn3.114)
8. Hansen BK, Bekkevold D, Clausen LW, Nielsen EE. 2018 The sceptical optimist: challenges and perspectives for the application of environmental DNA in marine fisheries. *Fish Fish*. **19**, 751–768. (doi:10.1111/faf.12286)
9. Scriver M, Zaiko A, Pochon X, von Ammon U. 2023 Harnessing decay rates for coastal marine biosecurity applications: a review of environmental DNA and RNA fate. *Environ. DNA* **5**, 960–972. (doi:10.1002/edn3.405)
10. Harrison JB, Sunday JM, Rogers SM. 2019 Predicting the fate of eDNA in the environment and implications for studying biodiversity. *Proc. R. Soc. B* **286**, 20191409. (doi:10.1098/rspb.2019.1409)
11. Thomsen PF, Kielgast J, Iversen LL, Møller PR, Rasmussen M, Willerslev E. 2012 Detection of a diverse marine fish fauna using environmental DNA from seawater samples. *PLoS One* **7**, e41732. (doi:10.1371/journal.pone.0041732)
12. Blackman R *et al*. 2024 Environmental DNA: the next chapter. *Mol. Ecol*. **33**, e17355. (doi:10.1111/mec.17355)
13. Murakami H *et al*. 2019 Dispersion and degradation of environmental DNA from caged fish in a marine environment. *Fish. Sci*. **85**, 327–337. (doi:10.1007/s12562-018-1282-6)

14. Goldberg CS, Strickler KM, Fremier AK. 2018 Degradation and dispersion limit environmental DNA detection of rare amphibians in wetlands: increasing efficacy of sampling designs. *Sci. Total Environ*. **633**, 695–703. (doi:10.1016/j.scitotenv.2018.02.295)
15. Dunker KJ, Sepulveda AJ, Massengill RL, Olsen JB, Russ OL, Wenburg JK, Antonovich A. 2016 Potential of environmental DNA to evaluate northern pike (*Esox lucius*) eradication efforts: an experimental test and case study. *PLoS One* **11**, e0162277. (doi:10.1371/journal.pone.0162277)
16. Brys R, Haegeman A, Halfmaerten D, Neyrinck S, Staelens A, Auwerx J, Ruttink T. 2021 Monitoring of spatiotemporal occupancy patterns of fish and amphibian species in a lentic aquatic system using environmental DNA. *Mol. Ecol*. **30**, 3097–3110. (doi:10.1111/mec.15742)
17. Eichmiller JJ, Bajer PG, Sorensen PW. 2014 The relationship between the distribution of common carp and their environmental DNA in a small lake. *PLoS One* **9**, e112611. (doi:10.1371/journal.pone.0112611)
18. Shogren AJ, Tank JL, Andruszkiewicz E, Olds B, Mahon AR, Jerde CL, Bolster D. 2017 Controls on eDNA movement in streams: transport, retention, and resuspension. *Sci. Rep.* **7**, 5065. (doi:10.1038/s41598-017-05223-1)
19. Nukazawa K, Hamasuna Y, Suzuki Y. 2018 Simulating the advection and degradation of the environmental DNA of common carp along a river. *Environ. Sci. Technol.* **52**, 10562–10570. (doi:10.1021/acs.est.8b02293)
20. Shogren AJ, Tank JL, Egan SP, Bolster D, Riis T. 2019 Riverine distribution of mussel environmental DNA reflects a balance among density, transport, and removal processes. *Freshw. Biol*. **64**, 1467–1479. (doi:10.1111/fwb.13319)
21. Jo T, Yamanaka H. 2022 Meta-analyses of environmental DNA downstream transport and deposition in relation to hydrogeography in riverine environments. *Freshw. Biol*. **67**, 1333–1343. (doi:10.1111/fwb.13920)
22. Pont D *et al*. 2018 Environmental DNA reveals quantitative patterns of fish biodiversity in large rivers despite its downstream transportation. *Sci. Rep*. **8**, 10361. (doi:10.1038/s41598-018-28424-8)
23. Deiner K, Altermatt F. 2014 Transport distance of invertebrate environmental DNA in a natural river. *PLoS One* **9**, e88786. (doi:10.1371/journal.pone.0088786)
24. Caza-Allard I, Laporte M, Côté G, April J, Bernatchez L. 2022 Effect of biotic and abiotic factors on the production and degradation of fish environmental DNA: an experimental evaluation. *Environ. DNA* **4**, 453–468. (doi:10.1002/edn3.266)
25. Ely T, Barber PH, Man L, Gold Z. 2021 Short-lived detection of an introduced vertebrate eDNA signal in a nearshore rocky reef environment. *PLoS One* **16**, e0245314. (doi:10.1371/journal.pone.0245314)
26. Port JA, O'Donnell JL, Romero-Maraccini OC, Leary PR, Litvin SY, Nickols KJ, Yamahara KM, Kelly RP. 2016 Assessing vertebrate biodiversity in a kelp forest ecosystem using environmental DNA. *Mol. Ecol*. **25**, 527–541. (doi:10.1111/mec.13481)
27. Jeunen GJ, Knapp M, Spencer HG, Lamare MD, Taylor HR, Stat M, Bunce M, Gemmell NJ. 2019 Environmental DNA (eDNA) metabarcoding reveals strong discrimination among diverse marine habitats connected by water movement. *Mol. Ecol. Resour*. **19**, 426–438. (doi:10.1111/1755-0998.12982)
28. Shea MM, Boehm AB. 2024 Environmental DNA (eDNA) metabarcoding differentiates between micro-habitats within the rocky intertidal. *Environ. DNA* **6**, e521. (doi:10.1101/2023.08.03.551543)
29. Baetscher DS, Pochardt MR, Barry PD, Larson WA. 2024 Tide impacts the dispersion of eDNA from nearshore net pens in a dynamic high-latitude marine environment. *Environ. DNA* **6**, e533. (doi:10.1002/edn3.533)
30. West KM, Stat M, Harvey ES, Skepper CL, DiBattista JD, Richards ZT, Travers MJ, Newman SJ, Bunce M. 2020 eDNA metabarcoding survey reveals fine-scale coral reef community variation across a remote, tropical island ecosystem. *Mol. Ecol*. **29**, 1069–1086. (doi:10.1111/mec.15382)
31. Kelly RP, Gallego R, Jacobs-Palmer E. 2018 The effect of tides on nearshore environmental DNA. *PeerJ* **6**, e4521. (doi:10.7717/peerj.4521)
32. Gallego A. 2011 Biophysical models: an evolving tool in marine ecological research. In *Modelling complex ecological dynamics* (eds F Jopp, H Reuter, B Breckling), pp. 279–289. Berlin, Germany: Springer. (doi:10.1007/978-3-642-05029-9_20)
33. Swearer SE, Treml EA, Shima JS. 2019 A review of biophysical models of marine larval dispersal. *J. Oceanogr. Mar. Biol.* **7**, 325–356. (doi:10.1201/9780429026379-7)
34. Aleynik D, Adams T, Davidson K, Dale A, Porter M, Black K, Burrows M. 2018 Biophysical modelling of marine organisms: fundamentals and applications to management of coastal waters. In *Environmental management of marine ecosystems* (eds Md Nazrul Islam, SE Jørgensen), pp. 65–98. Boca Raton, FL: CRC Press. (doi:10.1201/9781315153933-3)
35. Ellis MR *et al*. 2022 Detecting marine pests using environmental DNA and biophysical models. *Sci. Total Environ*. **816**, 151666. (doi:10.1016/j.scitotenv.2021.151666)
36. Andruszkiewicz EA, Koseff JR, Fringer OB, Ouellette NT, Lowe AB, Edwards CA, Boehm AB. 2019 Modeling environmental DNA transport in the coastal ocean using Lagrangian particle tracking. *Front. Mar. Sci.* **6**, 477. (doi:10.3389/fmars.2019.00477)
37. Kutti T, Johnsen IA, Skaar KS, Ray JL, Husa V, Dahlgren TG. 2020 Quantification of eDNA to map the distribution of cold-water coral reefs. *Front. Mar. Sci.* **7**, 446. (doi:10.3389/fmars.2020.00446)
38. Pastor Rollan A, Sherman CDH, Ellis MR, Tuohey K, Vennell R, Foster-Thorpe C, Treml EA. 2024 Current trends in biophysical modeling of eDNA dynamics for the detection of marine species. *Environ. DNA* **6**, e70021. (doi:10.1002/edn3.70021)
39. Richardson MF, Sherman CDH, Lee RS, Bott NJ, Hirst AJ. 2016 Multiple dispersal vectors drive range expansion in an invasive marine species. *Mol. Ecol*. **25**, 5001–5014. (doi:10.1111/mec.13817)
40. Fukaya K *et al*. 2021 Estimating fish population abundance by integrating quantitative data on environmental DNA and hydrodynamic modelling. *Mol. Ecol*. **30**, 3057–3067. (doi:10.1111/mec.15530)
41. Morrissey S, Jerry D, Kingsford M. 2024 Use of eDNA to test hypotheses on the ecology of *Chironex fleckeri* (Cubozoa). *Mar. Ecol. Prog. Ser*. **728**, 25–41. (doi:10.3354/meps14507)
42. Morrissey SJ, Jerry DR, Kingsford MJ. 2024 Use of eDNA to determine source locations of deadly jellyfish (Cubozoa) in an open coastal system. *Coasts* **4**, 198–212. (doi:10.3390/coasts4010011)
43. Morrissey SJ, Jerry DR, Kingsford MJ. 2022 Genetic detection and a method to study the ecology of deadly cubozoan jellyfish. *Diversity* **14**, 1139. (doi:10.3390/d14121139)
44. Kingsford MJ, Schlaefer JA, Morrissey SJ. 2021 Population structures and levels of connectivity for scyphozoan and cubozoan jellyfish. *Diversity* **13**, 174. (doi:10.3390/d13040174)
45. Kingsford MJ, Mooney CJ. 2014 The ecology of box jellyfishes (Cubozoa). In *Jellyfish blooms* (eds KA Pitt, CH Lucas), pp. 267–302. Dordrecht, The Netherlands: Springer. (doi:10.1007/978-94-007-7015-7_12)
46. Kingsford MJ, Becken S, Bordehore C, Fuentes VL, Pitt KA, Yangihara AA. 2018 Empowering stakeholders to manage stinging jellyfish: a perspective. *Coast. Manage.* **46**, 1–18. (doi:10.1080/08920753.2018.1405326)
47. Kingsford MJ, Seymour JE, O'Callaghan MD. 2012 Abundance patterns of cubozoans on and near the Great Barrier Reef. *Hydrobiologia* **690**, 257–268. (doi:10.1007/s10750-012-1041-0)
48. Gordon MR, Seymour JE. 2009 Quantifying movement of the tropical Australian cubozoan *Chironex fleckeri* using acoustic telemetry. *Hydrobiologia* **616**, 87–97. (doi:10.1007/s10750-008-9594-7)

49. Lambrechts J, Hanert E, Deleersnijder E, Bernard PE, Legat V, Remacle JF, Wolanski E. 2008 A multi-scale model of the hydrodynamics of the whole Great Barrier Reef. *Estuar. Coast. Shelf Sci*. **79**, 143–151. (doi:10.1016/j.ecss.2008.03.016)
50. Littlefair JE, Hrenchuk LE, Blanchfield PJ, Rennie MD, Cristescu ME. 2021 Thermal stratification and fish thermal preference explain vertical eDNA distributions in lakes. *Mol. Ecol*. **30**, 3083–3096. (doi:10.1111/mec.15623)
51. Schlaefer JA, Wolanski E, Lambrechts J, Kingsford MJ. 2021 Behavioural and oceanographic isolation of an island-based jellyfish (*Copula sivickisi*, Class Cubozoa) population. *Sci. Rep*. **11**, 11. (doi:10.1038/s41598-021-89755-7)
52. Kessler WS, Cravatte S. 2013 Mean circulation of the Coral Sea. *J. Geophys. Res*. **118**, 6385–6410. (doi:10.1002/2013jc009117)
53. Wolanski E, Kingsford M, Lambrechts J, Marmorino G. 2024 The physical oceanography of the Great Barrier Reef: a review. In *Oceanographic processes of coral reefs* (eds MJ Kingsford, E Wolanski), pp. 9–34. Boca Raton, FL: CRC Press. (doi:10.1201/9781003320425-3)
54. Herzfeld M. 2016 *EReefs marine modelling: final report*. Hobart, Australia: CSIRO.
55. Su CH *et al*. 2019 BARRA v1.0: the Bureau of Meteorology Atmospheric high-resolution Regional Reanalysis for Australia. *Geosci. Model Dev.* **12**, 2049–2068. (doi:10.5194/gmd-2018-277)
56. Wolanski E, De Le Court M, Lambrechts J, Kingsford M. 2024 Mechanisms enabling the self-recruitment of passive larvae in the Great Barrier Reef. *Estuar. Coast. Shelf Sci.* **309**, 108976. (doi:10.1016/j.ecss.2024.108976)
57. de Brye B, de Brauwere A, Gourgue O, Kärnä T, Lambrechts J, Comblen R, Deleersnijder E. 2010 A finite-element, multi-scale model of the Scheldt tributaries, river, estuary and ROFI. *Coast. Eng*. **57**, 850–863. (doi:10.1016/j.coastaleng.2010.04.001)
58. Schlaefer J, Carter A, Choukroun S, Coles R, Critchell K, Lambrechts J, Rasheed M, Tol S, Grech A. 2022 Marine plant dispersal and connectivity measures differ in their sensitivity to biophysical model parameters. *Environ. Model. Softw*. **149**, 105313. (doi:10.1016/j.envsoft.2022.105313)
59. BoM. 2024 Climate data. See http://www.bom.gov.au/climate/data/.
60. Andutta FP, Kingsford MJ, Wolanski E. 2012 'Sticky water' enables the retention of larvae in a reef mosaic. *Estuar. Coast. Shelf Sci*. **101**, 54–63. (doi:10.1016/j.ecss.2012.02.013)
61. Lázaro BJ, Lasheras JC. 1989 Particle dispersion in a turbulent, plane, free shear layer. *Phys. Fluids* **1**, 1035–1044. (doi:10.1063/1.857394)
62. Strickland JK, Pitt KA, Kingsford MJ, Morrissey SJ, Jerry DR. 2025 Real-time PCR assay and environmental DNA workflow for detecting Irukandji jellyfish, *Malo bella* (Cubozoa). *Environ. DNA* **7**, e70071. (doi:10.1002/edn3.70071)
63. Mooney CJ, Kingsford MJ. 2017 Discriminating populations of medusae (*Chironex fleckeri*, Cubozoa) using statolith microchemistry. *Mar. Freshw. Res*. **68**, 1144–1152. (doi:10.1071/MF16104)
64. Brown TW. 1973 *Chironex fleckeri: distribution and movements around Magnetic Island, north Queensland*. Townsville, Australia: James Cook University.
65. Morrissey SJ, Yanagihara AA, Kingsford MJ. 2020 Utility of statolith elemental chemistry as a proxy for temperature to elucidate the movements of the Irukandji jellyfish species *Alatina alata*. *Mar. Biol.* **167**, 134. (doi:10.1007/s00227-020-03752-4)
66. Barnes MA, Turner CR, Jerde CL, Renshaw MA, Chadderton WL, Lodge DM. 2014 Environmental conditions influence eDNA persistence in aquatic systems. *Environ. Sci. Technol*. **48**, 1819–1827. (doi:10.1021/es404734p)
67. Brandão-Dias PFP *et al*. 2023 Suspended materials affect particle size distribution and removal of environmental DNA in flowing waters. *Environ. Sci. Technol.* **57**, 13161–13171. (doi:10.1021/acs.est.3c02638)
68. Jo T, Arimoto M, Murakami H, Masuda R, Minamoto T. 2019 Particle size distribution of environmental DNA from the nuclei of marine fish. *Environ. Sci. Technol.* **53**, 9947–9956. (doi:10.1021/acs.est.9b02833)
69. Brandão-Dias PFP *et al*. 2023 Particle size influences decay rates of environmental DNA in aquatic systems. *Mol. Ecol. Resour*. **23**, 756–770. (doi:10.1111/1755-0998.13751)
70. Williams MA, O'Grady J, Ball B, Carlsson J, de Eyto E, McGinnity P, Jennings E, Regan F, Parle-McDermott A. 2019 The application of CRISPR-Cas for single species identification from environmental DNA. *Mol. Ecol. Resour*. **19**, 1106–1114. (doi:10.1111/1755-0998.13045)
71. Morrissey S. 2025 Estimating transport and detectability of Chironex fleckeri eDNA in an open coastal bay. [Data set]. Zenodo. (doi:10.5281/zenodo.17773092)
72. Morrissey SJ, Schlaefer JA, Jerry D, Kingsford M. 2026 Supplementary material from: Estimating transport and detectability of Chironex fleckeri eDNA in an open coastal bay. Figshare. (doi:10.6084/m9.figshare.c.8262531)